THE JOURNAL OF PHYSICAL CHEMISTRY C

Article

pubs.acs.org/JPCC

# Revealing Ordered Polymer Packing during Freeze-Drying Fabrication of a Bulk Heterojunction Poly(3-hexylthiophene-2,5-diyl):[6,6]-Phenyl-C61-butyric Acid Methyl Ester Layer: In Situ Optical Spectroscopy, Molecular Dynamics Simulation, and X-ray Diffraction

Yu-Bing Lan,[†,‡,§] Pin-Hao Sher,[§] Cheng-Kuang Lee,[▽] Chun-Wei Pao,*[,∥] Cheng-Si Tsao,*[,⊥,○] Yu-Ching Huang,[⊥] Ping-Tsung Huang,[#] Chih-I Wu,[‡] and Juen-Kai Wang*[,†,§]

[†]Center for Condensed Matter Sciences and [‡]Graduate Institute of Photonics and Optoelectronics, National Taiwan University, Taipei 10617, Taiwan

[§]Institute of Atomic and Molecular Sciences, Academia Sinica, Taipei 10617, Taiwan

[∥]Research Center for Applied Sciences, Academia Sinica, Taipei 11529, Taiwan

[⊥]Institute of Nuclear Energy Research, Taoyuan 32546, Taiwan

[#]Department of Chemistry, Fu-Jen Catholic University, Taipei 24205, Taiwan

[▽]Material and Chemical Research Laboratories, Industrial Technology Research Institute, Hsinchu 31040, Taiwan

[○]Department of Materials Science and Engineering, National Taiwan University, Taipei 10617, Taiwan

*Supporting Information*

**ABSTRACT:** Formation of ordered poly(3-hexylthiophene-2,5-diyl) (P3HT) molecular stacking during the freeze-drying process is tracked with in situ spectroscopy of Raman scattering, absorption, and photoluminescence. Raman spectra of pristine P3HT dissolved in 1,2-dichlorobenzene show that P3HT polymers undergo drastic ordered aggregation upon being lower than 0 °C, at which the solubility of P3HT is reached, as evidenced by the emergence of pronounced red-shifted, narrow Raman peaks (1422 and 1435 $cm^{-1}$) caused by intermolecular coupling. The absorption and photoluminescence spectra bear similar temperature dependence as the results of Raman. Aggregation of P3HT is further confirmed by coarse-grained molecular dynamics simulation showing the enhanced order parameters of distance and orientation between P3HT chains upon cooling. The incorporation of [6,6]-phenyl-C61-butyric acid methyl ester (PCBM) does not significantly alter the P3HT packing configuration, as verified by nearly identical Raman features observed in P3HT:PCBM mixing solution upon cooling. While optical spectroscopy and MD simulation portrayed the short-range order of P3HT aggregates, grazing-incident X-ray diffraction exposed the long-range order by the pronounced diffraction spots corresponding to the lamellar stacking of P3HT. This study demonstrates the ability of Raman spectroscopy to reveal the short-range order of polymer packing, while the in situ monitoring illustrates that the ability of freeze-drying to separate molecular aggregation from solvent removal thus is advantageous for photovoltaic device fabrication without resorting to trial and error.

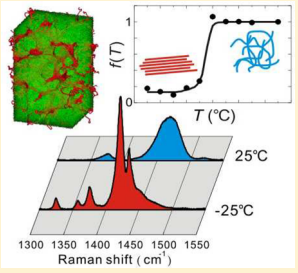


## INTRODUCTION

Among promising new-generation solar-cell technologies,[1,2] organic photovoltaics attract great attention because of their low Eco-indictor 99[3] values—accounting for ecosystem-quality damage (toxic emission and land-use damage), human health damage, and resources—and short energy payback time, compared with conventional photovoltaic technologies.[4] The fundamental processes underlying organic photovoltaic devices are 5-fold: (1) exciton creation by light absorption, (2) exciton diffusion, (3) exciton dissociation, (4) charge conduction, and (5) charge collection.[1] Among them, processes (2) and (4) critically depend on molecular alignment in connected nanometer-scaled morphology, because ordered molecular stacking would facilitate charge hopping via preferential intermolecular coupling and connected nanometer-scaled morphology—the bulk heterojunction (BHJ) concept—would allow for efficient conduction channels of separated electrons and holes to their respective electrodes.[5] There have been several successful approaches developed to realize such control on both microscopic and mesoscopic scales simultaneously, such as thermal annealing[6] and solvent annealing,[7] to name two well-known ones. The former promptly removes residual solvent from the wet blended film and simultaneously enables molecular stacking and connected nanomorphology formation via heating, while the solvent evaporates slowly at room temperature in an enclosed environment in the latter case such that the molecules in the active layer could progressively form ordered stacking and nanometer-scaled connected

**Received:** February 21, 2017
**Revised:** June 5, 2017
**Published:** June 5, 2017






DOI: 10.1021/acs.jpcc.7b01679
J. Phys. Chem. C 2017, 121, 14826−14834

networks. Despite these achievements, attaining high photovoltaic performance with newly synthesized molecules still relies greatly on trial and error, because the required delicate balance among many physical processes at the molecular and nanometer levels involved would vary greatly, making searching for the optimal fabrication process rather time-consuming, if not impossible.

Recently, a freeze-drying method has been proposed to manufacture BHJ polymer solar cells that generate 25% higher power conversion efficiency than those fabricated using the conventional thermal annealing method.[8] The method starts with cooling the polymer solution below the triple point of the solvent while promoting molecular aggregation, which is then followed by solvent sublimation in high vacuum and finally ends with the remaining polymer scaffold being heated back to room temperature. The essence of the freeze-drying method is to separate the formation of ordered molecular aggregates from the solvent removal process. This scenario is however created without experimental verification, particularly lacking the direct revelation of the aforementioned happenings.

Using the prototypical blended system of poly(3-hexylthiophene-2,5-diyl) (P3HT) and [6,6]-phenyl-C61-butyric acid methyl ester (PCBM) with 1,2-dichlorobenzene (*o*-DCB) as solvent, this study discloses the evolution of P3HT molecular stacking during the freeze-drying process by in situ spectroscopy methods of Raman scattering, absorption, and photoluminescence (PL) and molecular dynamic simulation and confirms the findings with ex-situ X-ray diffraction. The results show that P3HT polymers in either pristine P3HT or P3HT:PCBM blends undergo dramatic ordered aggregation between 0 and −5 °C as their solubility in *o*-DCB is approached, giving significant red-shifted absorption, and the resultant dried film at room temperature contains a large quantity of P3HT domains with high stacking order compared with the film made by conventional thermal annealing. This work demonstrates for the first time, to our knowledge, Raman spectroscopy as a powerful tool to reveal short-range order in molecular aggregates, which is essential to favorable charge conduction in organic semiconductors.

## MATERIALS AND METHODS

**Sample Preparation.** P3HT (region-regularity 93%) was purchased from Rieke Metals with an average molecular weight of 53 kg/mol. PCBM was acquired from Solenne (99.5% purity). Solutions of P3HT (1 wt %) and P3HT:PCBM (1:0.8 in wt %) were prepared in spectral grade *o*-DCB by stirring at 500 rpm and 50 °C overnight. All pristine P3HT and P3HT:PCBM samples used in the optical studies during dynamical cooling were prepared by drop-casting 20 μL of the sample solution onto fused-silica substrates. The corresponding P3HT:PCBM samples exposed to the other conditions—after a freeze-dry cycle in a vacuum and subsequent annealing and after conventional direct annealing at 150 °C for 5 min—were prepared by spin-coating at 1000 rpm for 10 s. The samples used in the in situ optical studies were directly mounted in a cryostat inside a nitrogen-gas-filled glovebox (humidity ∼ 33 ppm; $[O_2]$ ∼ 194 ppm). A more detailed description is given below. On the other hand, the sample prepared by spin-coating and direct annealing used for comparison was encapsulated with a fused-silica cover glass in the same glovebox.

**In Situ Optical Spectroscopy.** In situ optical experiments were performed in an optical microscope setup combined with a temperature-controlled open-cycle cryostat system (RC102-CFM, CIA). Its schematic is shown in Figure S1 of the Supporting Information (SI). The samples prepared either by drop-casting or spin-coating were attached on the sample stage of the cryostat with conductive silver adhesive in the same nitrogen-gas-filled glovebox mentioned above. The cryostat chamber was then sealed after placing five additional 20-μL droplets of *o*-DCB beside the sample, thus creating a saturated solvent vapor pressure that minimized solvent evaporation from the sample in the sealed chamber during the experiments. The constant content of *o*-DCB in the sample was verified by the invariant Raman peak intensity of *o*-DCB before solvent sublimation. To know the actual temperature of the sample, a temperature calibration procedure was adopted to determine the temperature difference between the sample site and the sample stage where the temperature sensor is located: (1) the Raman shift of a small piece of Si wafer attached to a bare fused-silica substrate was monitored as a function of the reading of the temperature sensor and (2) the sample temperature was determined by referring to the known temperature-dependent Raman shift of silicon.[9] The thermal equilibrium of the sample at each designated temperature was confirmed by continuously acquiring the optical spectra until no further variation was observed. For Raman measurements, a single-mode diode laser emitting at 785 nm acted as the excitation source to avoid the fluorescence background from P3HT. The laser beam was focused by a 10× micro-objective lens at a location 200 μm below the top surface of the drop-cast samples in the cryostat. The scattered radiation was collected backward with the same objective lens and sent to an 80 cm spectrometer plus a liquid nitrogen cooled charge-coupled device (CCD) for spectral recording. The spectral calibration was done with an Hg−Ne lamp. The spectral resolution was 3 $cm^{-1}$ and the spectral error was less than 0.1 $cm^{-1}$. The typical acquisition time ranged from 10 to 30 s. The laser irradiation power was set at 2.5 mW to avoid photodegradation. Photoluminescence spectra were collected using the same objective lens. The excitation source for the photoluminescence experiment was a CW frequency-doubled diode-pumped Nd:YAG laser emitting at 532 nm, while the irradiation source for the absorption experiment, impinging the sample from the bottom of the cryostat, was a halogen lamp filtered with an infrared-absorbing filter to avoid unwanted heating. The spectrometer used for both the photoluminescence and absorption experiments was a 14 cm spectrometer (MicroHR, Horiba) with a 600 grooves/mm grating. A thermoelectric-cooled CCD (Newton 920, Andor) was used as the multichannel detector to acquire the photoluminescence spectra. The spectral response of the system had been calibrated with a NIST-traceable light source. On the other hand, a silicon photodiode served as the single-channel detector for the absorption experiment. The uniformity of the sample spectra was assured by the similarity among five spectra acquired at different sample locations. The optical experiments done on the thin-film samples followed the same procedure as stated above, except that the laser beam was focused on the top surface of the samples.

**GIXRD.** Grazing-incidence X-ray diffraction (GIXRD) measurement was performed using an in-house X-ray scattering instrument (Nanostar, Bruker) equipped with a rotating Cu anode irradiated with a 2.5 kW electron beam, a two-dimensional (2D) image plate as the detector, and a three-pinhole system for alignment. The samples for GIXRD experiments were spin-coated on Si(111) substrates followed by the freeze-drying process. The grazing angle of the GIXRD



DOI: 10.1021/acs.jpcc.7b01679
J. Phys. Chem. C 2017, 121, 14826−14834

measurement was aligned to be 0.2° ± 0.002°, for penetrating through the whole active layer.[10] The previous studies reported that the GIXRD patterns produced by the active layer are unaffected by the use of silicon and ITO/PEDOT:PSS substrates.[11] The in-plane GIXRD profiles as a function of scattering vector $Q_X$ were deduced from the 2D GIXRD patterns along the in-plane direction (parallel to the substrate or film surface, defined as the $X$ direction). The out-of-plane GIXRD profiles were extracted from the 2D GIXRD patterns along the out-of-plane direction (perpendicular to the substrate and film surface, defined as the $Z$ direction) and were expressed as a function of scattering vector $Q_Z$.

**Molecular Dynamic Simulation.** The methods of multiscale molecular dynamics (MD) simulations used in this study included coarse-grained (CG) molecular simulations based on atomistic molecular dynamics (AMD) simulations, backmapping techniques, and morphology evaluation schemes.[12] To build the CG model, each P3HT repeated unit was coarse-grained into a CG bead centered at the mass center of the thiophene ring. For *o*-DCB molecules, the whole molecule was coarse-grained into one CG bead centered at the mass center of the *o*-DCB molecule. The CG force fields between CG particles were fitted to reproduce the structural properties of P3HT and *o*-DCB blends. The CG interaction between intramolecular CG degrees of freedom (namely, CG bond length, angle, and dihedral) were fitted such that the distribution functions of these CG degrees of freedom from the CG force field can reproduce those from all-atom MD simulations of smaller systems of interests. For intermolecular CG interactions, the CG force fields were fitted such that the radial distribution functions (RDFs) of CG beads from the fitted CG force field can reproduce those RDFs from all-atom MD simulations. The details of fitting CG force fields can be found elsewhere.[12,13] The CGMD simulations were carried out using NAMD2.[14]

## RESULTS AND DISCUSSION

**Characterization and Simulation during Cooling.** In situ optical spectroscopic measurements were performed on a droplet of pristine P3HT dissolved in *o*-DCB (1 wt %) in a cryostat system. Cooling the liquid droplet from room temperature to a series of designated temperatures emulated the dynamical cooling process. Spectra of Raman scattering, absorption, and photoluminescence were acquired at those temperatures to monitor the evolution of vibrational modes and electronic transitions, corresponding to the progressing state of molecular packing. Figure 1a shows such Raman spectra from 1300 to 1550 $cm^{-1}$, where the vibrational modes of the thiophene ring reside,[15,16] of pristine P3HT dissolved in *o*-DCB at four characteristic temperatures (25, 0, −5, and −25 °C). The spectra of finer temperature variations are shown in Figure S2 in the Supporting Information. Notably, the spectrum at 25 °C exhibits a broad peak centered around 1470 $cm^{-1}$ and a small peak at 1376 $cm^{-1}$, corresponding to the C═C and C−C stretches of the thiophene ring of P3HT, respectively.[15,16] The broad width of the 1470 $cm^{-1}$ peak reflects that the conformation of the fully dissolved, and thus relaxed, isolated P3HT molecules in the solution possibly undergoes great variation caused by countlessly different solvent environments, yielding a large inhomogeneous distribution in their conformation. For the temperature quenched to less than 0 °C, two prominent peaks at 1422 and 1435 $cm^{-1}$ accompanied by two smaller peaks at 1325 and 1358 $cm^{-1}$ emerge, while the broad 1470 $cm^{-1}$ peak is reduced and the 1376 $cm^{-1}$ peak

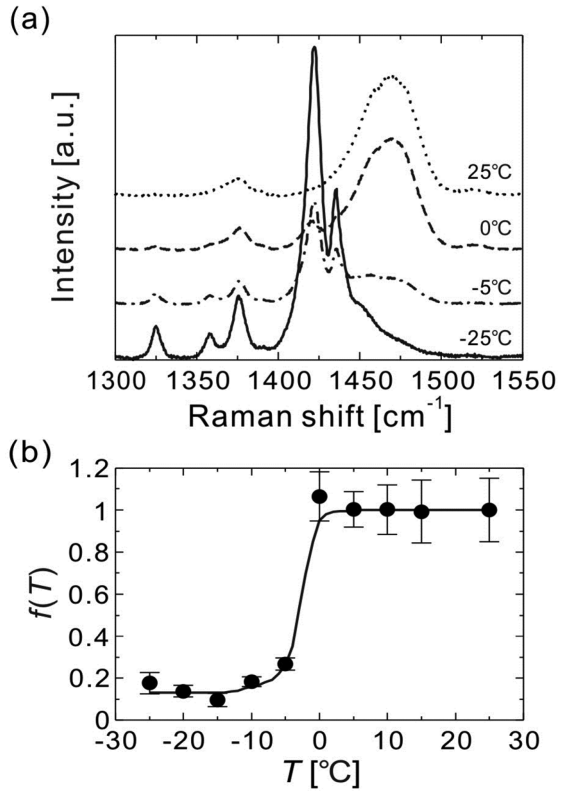


**Figure 1.** (a) Raman spectra of neat P3HT in *o*-DCB at 25 °C (dotted curve), 0 °C (dashed curve), −5 °C (dotted−dashed curve), and −25 °C (solid curve). (b) Fraction of isolated P3HT acquired from Raman spectra at different temperatures [$f(T)$]; see the text for its definition. The curve is a guide to the eyes.

becomes narrower and more intense. These unprecedented P3HT Raman features at the ultimate −25 °C are considerably narrow relative to the original two Raman features at room temperature. The possible causes of such a dramatic shift in the vibrational frequency as well as the new peaks at 1325 and 1358 $cm^{-1}$ are 2-fold: extended conjugation[16,17] and intermolecular coupling[17] predicted in previously simplified theoretical studies. First, with density functional theory (DFT), Tsoi et al. simulated the Raman spectrum of polythiophene in a helical structure with different dihedral angles between thiophene units.[16] On the basis of the simulation results, they ascribed the red-shifting of the C═C peak of regioregular P3HT film after thermal annealing to a more planar backbone conformation and therefore better ordering of regioregular P3HT molecules. More recently, Donohoo-Vallett and Bragg[18] revisited this problem with long-range-corrected functionals in DFT simulation and discovered that the red-shift of the C═C stretch frequency with increased order actually reflects balanced contributions of mechanical and quantum-mechanical (QM) effects on the C═C stretching frequency: The mechanical contribution originates from the fact that the stretching frequency of one-dimensional chain increases with its length, while the QM one engenders softened backbone stretches through nonlocal $\pi$-electron interactions in extended conjugation length (effective conjugation coordinate theory) owing to structural ordering. The observed red-shifting in the C═C stretches in Figure 1a suggests that the QM effect in the extended conjugation length prevails in the shifted Raman signature of ordered P3HT aggregates formed below 0 °C. Besides, Milani et al.[17] performed experimental and simulation


DOI: 10.1021/acs.jpcc.7b01679
J. Phys. Chem. C 2017, 121, 14826−14834

studies of the intermolecular interaction effect on Raman spectra of polythiophene—a polyconjugated molecule—and found that its C═C stretch frequency is red-shifted by an intermolecular dipole−dipole interaction. In our separate ongoing effort, we investigate the Raman spectrum of crystalline P3HT in different packing configurations (orientations and separations) with first-principle calculations. The preliminary result shows that the Raman signatures of a specific energy-minimum packing arrangement of P3HT exhibit almost identical features as the Raman spectrum of P3HT in *o*-DCB at −25 °C and are sensitive to the interchain separation, suggesting that the intermolecular interaction can play a role. Given the discussion above, we thus assign the two peaks at 1422 and 1435 $cm^{-1}$ to the C═C stretch from ordered packing of P3HT that is compared to the isolated and disordered P3HT signified by the broad Raman feature at 1470 $cm^{-1}$.

We note that Louarn and co-workers observed alike red-shifting in the Raman and absorption spectra of poly(3-decylthiophene) (P3DT) under voltage bias.[19] However, three spectral distinctions exist between their findings and ours. First, the 1445 $cm^{-1}$ Raman peak (symmetric C═C stretching mode) portrayed in the charged P3DT is significantly broadened, in contrast to the splitting and narrowing of the same Raman peak observed at −25 °C in our sample. Second, the absorption spectrum of the charged P3DT displays a smaller vibronic feature that is inconsistent with the low-temperature spectrum of P3HT, which exhibits pronounced vibronic features separated by 170 meV. Third, the absorption spectrum of charged P3DT is much broader and extends further to the near-IR than that of P3HT at −25 °C. Furthermore, with the copper coldfinger of the cryostat grounded, several confirmatory experiments were performed with different substrates, (1) a conductive aluminum holder, (2) semiconducting silicon substrates, and (3) insulating fused-silica substrates, and all of them showed the same Raman and photoluminescence features at −25 °C. Therefore, anomalous charge injection in our case can be ruled out. Charging by chemical impurities should be minimal, as the solvents used are purified optical grade. Even if a small amount of impurities existed, their effect would remain constant and should not emerge only at low temperatures. Another suspected possibility−polarons produced via optical excitation and subsequently delocalized—can be excluded, since the excitation photon energy of the Raman experiment (1.58 eV, corresponding to 785 nm) is away from the lowest energy required for optical excitation (2.2 and 1.75 eV for isolated and aggregated P3HT, respectively). The spectral evidence and the experimental efforts above therefore conclude that our observed Raman spectra of P3HT at low temperatures resulted from aggregation of P3HT.

To facilitate the quantitative analysis of these Raman features, the spectra were fitted with multiple Gaussian peaks at respective nominal frequencies (Figure S3, SI). The integrated intensity over the extracted broad 1470 $cm^{-1}$ peak at each temperature, $S_i(T)$, was determined. The ratio of $f(T) = S_i(T)/S_i(25°C)$ corresponds to the proportion of isolated P3HT and is plotted against temperature in Figure 1b. Note that the disordered P3HT isolates undergo a drastic decrease between 0 and −5 °C. As the solubility of P3HT in *o*-DCB at 0 °C is about 1%,[20] close to the concentration of dissolved P3HT in the sample, the P3HT molecules would start segregation as the temperature approaches 0 °C. According to the Raman data, it appears that the segregation ceases just below −5 °C and the proportion of isolated P3HT remains at <20% at the lower temperatures, even below the triple point of *o*-DCB ($T_{tp}$ = −17 °C).[21] This transition-typed behavior might be caused by the fact that the viscosity of liquid *o*-DCB increases significantly as its temperature approaches the freezing point[22]—the Stokes−Einstein relation.[23] The viscous solvent hinders the diffusion of isolated P3HT polymers and thus can halt the polymer segregation if the isolated P3HT polymers are too far apart at the temperature lower than −5 °C. The observed evolution in Raman spectroscopic signatures reveals the progression of P3HT aggregation in *o*-DCB during dynamical cooling, which would also be manifest from the in situ characterization with absorption and photoluminescence.

Molecular absorption and photoluminescence reflect optically allowed transitions between electronic states. If molecular aggregation does occur at low sample temperatures, intermolecular exciton coupling engendered by molecular aggregation will manifest itself as the emergence of low-energy peaks. Figure 2 shows the absorption and photoluminescence spectra

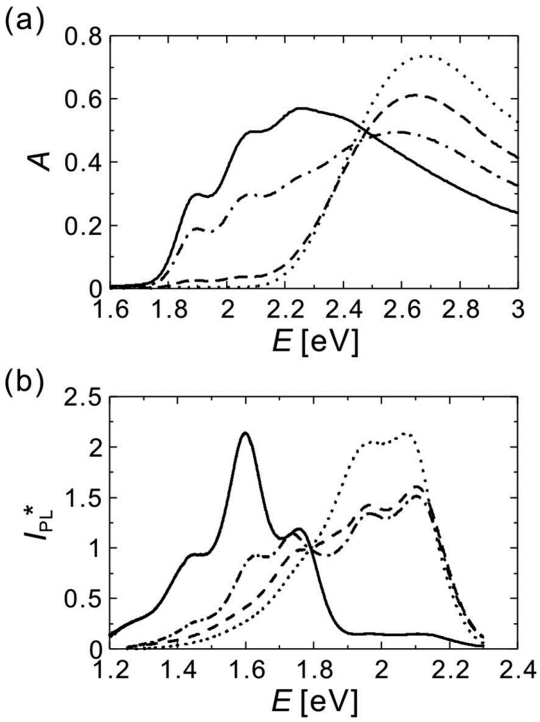


**Figure 2.** (a) In situ absorbance ($A$) and (b) PL spectra of neat P3HT in *o*-DCB at 25 °C (dotted curve), 0 °C (dashed curve), −5 °C (dotted−dashed curve), and −25 °C (solid curve). $I^*_{PL} = I_{PL}(E)/I_{PL}(1.79\ eV)$.

of 1 wt % P3HT in *o*-DCB at the same four temperatures (25, 0, −5, and −25 °C). Similarly, the spectra of finer temperature variation are shown in Figures S4 and S5 of the Supporting Information. Note that the absorption spectrum at 25 °C (Figure 2a) shows a single featureless band peaked at 2.68 eV and with a low-energy onset at ∼2.1 eV, which is in good agreement with the previous works.[24,25] At 0 °C, some absorption feature appears below the absorption onset energy. Such a feature becomes prominent at −5 °C, while the original high-energy absorption band decreases significantly. From −5 to −20 °C, the low-energy absorption feature continues increasing and presents at least two conspicuous vibronic bands peaked at 1.89 and 2.06 eV, while the high-energy


DOI: 10.1021/acs.jpcc.7b01679
J. Phys. Chem. C 2017, 121, 14826−14834

absorption feature decreases further (see Figure S4, SI). Finally, the absorption spectrum converges to the one at −25 °C. These emergent peaks (except the lowest peak at 1.89 eV) were similarly observed by Clark et al. for P3HT dissolved in isodurene and originate from intramolecular $\pi-\pi^*$ transitions.[24] They attributed them to the formation of P3HT H-aggregates. A model accounting for exciton−phonon coupling in different aggregation forms was developed to interpret the observed absorption and photoluminescence spectra. The 1.89 eV absorption peak was similarly observed in the case of P3HT crystallite by Rahimi et al.[26] and attributed to interchain exciton−vibration coupling at small interchain spacing. The missing low-energy feature in the study of Clark et al. could be due to the fact that their experiment was carried out above room temperature. The evolution in absorption shows good correspondence with that in photoluminescence in Figure 2b and Figure S5 (SI). The photoluminescence spectrum at 25 °C displays two clear vibronic features at 1.95 and 2.1 eV with the whole spectral range from ∼1.3 to ∼2.3 eV. At 0 °C, a spectral feature below ∼1.8 eV emerges, and the high-energy vibronic features decline. From −5 to −25 °C, the spectrum below 1.8 eV presents three conspicuous vibronic bands peaked at 1.45, 1.6, and 1.75 eV, while the spectrum above diminishes. These bands are associated with aggregated P3HT in the frozen solution. Besides the spectral change, the photoluminescence intensity at −25 °C is reduced to about 3 orders of magnitude smaller than that at room temperature.

In light of the findings from the Raman study above, two inferences can be made on the basis of the absorption and photoluminescence data. First, both emergent low-energy spectral signatures in absorption and photoluminescence below 0 °C are indicative of aggregation of P3HT, providing additional spectroscopic evidence corresponding to the observed sharp red-shifted Raman peaks in the same temperature range. Second, several previous experimental works have tried to separate disordered and ordered P3HT aggregates on the basis of the spectral signatures of absorption and photoluminescence[24,25,27] with use of Spano's aggregate model.[28,29] For example, Köhler's group[25] adopted the model to account for the vibronic features in the absorption, while leaving the high-energy absorption tail as "the residue." The unknown "residue" might cause uncertainty in the extracted Spano's parameters and likely results in the ambiguous determination of the aggregate proportion. The unequivocal distinction of the Raman spectra at different temperatures, on the other hand, can be readily realized owing to the intrinsic Gaussian-shaped profile of Raman peaks, providing direct quantitative information about the proportion of disordered P3HT. Accordingly, Raman spectroscopy exhibits two unique advantages in the context of studying molecular aggregates: (1) easy spectral analysis and (2) direct revelation of molecular packing with first-principle calculation.

The molecular aggregation of P3HT in *o*-DCB upon dynamical cooling was further investigated with coarse-grained molecular-dynamic (CGMD) simulations.[12,13,30,31] Figure 3a displays simulated snapshots of P3HT in *o*-DCB equilibrated at 25 and −25 °C. Note that the P3HT aggregates are formed at −25 °C while they are absent at 25 °C. After back-mapping them back to atomistic forms, the RDF of thiophene rings and their orientational order parameter[12,32] were evaluated at the same four temperatures as above. Two parameters are used to reveal the packing order of the P3HT aggregates in interchain distance and orientation from the simulation: (1) the height of

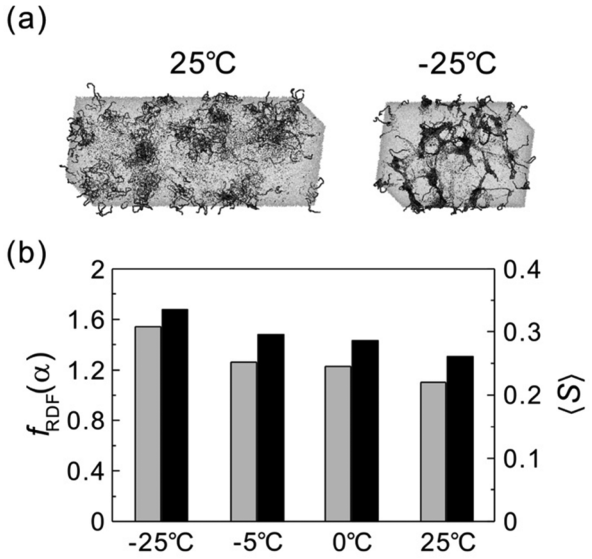


**Figure 3.** (a) Snapshots of CGMD simulation of P3HT in *o*-DCB equilibrating at 25 °C and at −25 °C. (b) Column charts of order parameters of distance and orientation, $f_{RDF}(\alpha)$ (gray columns) and $\langle S \rangle$ (black columns), respectively, of P3HT chains from the simulation at 25, 0, −5, and −25 °C.

the RDF of the smallest distance between thiophene rings, $f_{RDF}(\alpha)$, and (2) the mean local orientational order parameter of P3HT chains, $\langle S \rangle$. Figure S6 (SI) shows the schematic illustration of the distance between thiophenes in different P3HT chains, $r_{TP}$, and $f_{RDF}(r_{TP})$ at the four temperatures: the higher first peak of $f_{RDF}(r_{TP})$ implies higher degrees of thiophene $\pi-\pi$ stacking.[12] In the local orientational order parameters, P3HT chains are discretized into 10 nm subdomains, and the local orientational order parameter of the *j*th subdomain is computed by $S_j = \langle 3 \cos^2 \theta - 1 \rangle/2$, where $\theta$ is the angle between the bond vector of the P3HT backbone and the mean bond vectors in the *j*th subdomain (see Figure S7 in the Supporting Information for the schematic illustration of the definitions of $\theta$ and $S$ in the simulated ensemble at the four temperatures). By taking an average of $S_j$ values of all P3HT subdomains, we obtained the mean local orientational order parameter $\langle S \rangle$. Hence, high magnitudes of $f_{RDF}(\alpha)$ and $\langle S \rangle$ indicate a high degree of alignment of P3HT chains. As displayed in Figure 3b, it is evident that the lower the temperature is, the higher the degree of P3HT alignment is, demonstrating the same trend as the experimental findings in in situ optical spectroscopy.

The same in situ spectroscopic study was then undertaken in the case of mixed P3HT with PCBM (1:0.8 in wt %) in *o*-DCB during dynamical cooling. The Raman scattering and absorption spectral signatures of blended P3HT:PCBM samples (Figure 4) exhibit almost the same behaviors as that of neat P3HT. Since vibrational frequencies of organic molecules are known to be sensitive to short-range intermolecular coupling and therefore their aggregation condition in condensed phase, the close similarity in Raman spectra of pristine P3HT and the P3HT:PCBM blend suggests that the incorporated PCBM in the blend does not significantly alter the P3HT packing configuration between adjacent polymer chains owing to their comparably stronger mutual interaction than that between P3HT and PCBM. We note that its photoluminescence declined by between one-half and two-thirds in intensity and the spectral signature was altered


DOI: 10.1021/acs.jpcc.7b01679
J. Phys. Chem. C 2017, 121, 14826−14834

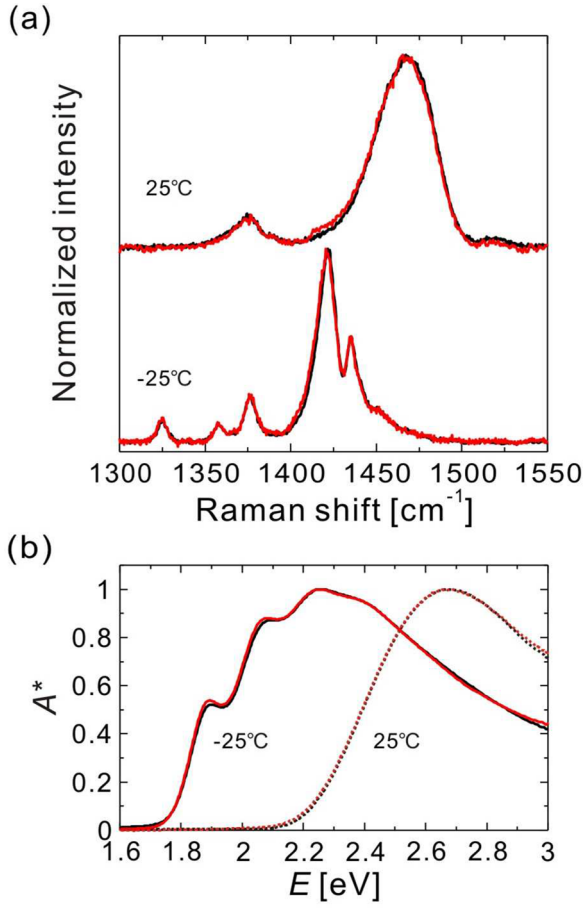


**Figure 4.** Comparisons of (a) Raman spectra and (b) absorption spectra of P3HT:PCBM (1:0.8) blend (red curve) with neat P3HT (black curve) both in *o*-DCB at 25 °C and −25 °C.

compared to that of the neat P3HT counterpart. One possible cause of such behavior is preferential binding of longer-chain P3HT with PCBM because of its larger collision cross-section with PCBM in *o*-DCB, resulting in lower intensity and differing spectrum of photoluminescence. The photoluminescence spectroscopy encounters two problems throughout the experiments. First, P3HT self-absorption—for example, the absorption and photoluminescence spectra of P3HT in *o*-DCB at −25 °C overlap from 1.8 to 2.2 eV—possibly distorts its own photoluminescence spectrum. Since the absorption spectrum of P3HT varies with temperature (Figure 2a), the photoluminescence signal at different wavelengths at different temperatures may come from different probing depths of the sample, making simple interpretation of the photoluminescence spectra rather difficult. Second, P3HT fluorescence is quenched by adjacent PCBM. Consequently, the majority of the photoluminescence would originate from P3HT chains not in contact with PCBM, and the spectrum is ill-representing the entire ensemble. Therefore, we will not discuss the photoluminescence spectra further in this report. Similarly, $f_{RDF}(\alpha)$ and $\langle S \rangle$ garnered from MD simulation for the P3HT:PCBM blend also exhibit almost identical features, as shown in Figure 3b. Such consistency in spectral signatures and MD simulation between neat P3HT and P3HT:PCBM blends is rational, in light of the immiscibility between P3HT and PCBM.[33] Given this fact, two subsequent questions naturally arise: (1) How does this extraordinary ordering in molecular packing during dynamical cooling affect the final ordering after solvent sublimation, sample warming, and further annealing, and (2) how is it compared with the sample prepared by the conventional thermal annealing method?

**Characterization during Solvent Sublimation and Heating.** Figure 5 shows the spectra of Raman scattering

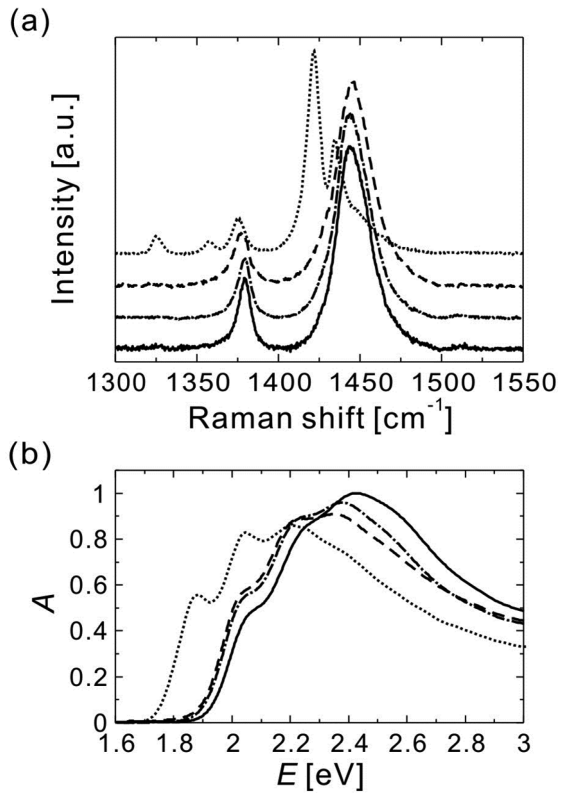


**Figure 5.** Spectra of (a) Raman scattering and (b) absorption of the P3HT:PCBM (1:0.8) film after dynamical cooling to −25 °C and solvent sublimation of <40 min (dotted curve), then after being heated to room temperature (dashed curve), and finally after thermal annealing at 150 °C for 5 min (dotted−dashed curve) and of the P3HT:PCBM (1:0.8) film after direct thermal annealing at 150 °C for 5 min (solid curve).

and absorption of the cooled P3HT:PCBM sample after solvent removal in vacuum, as evidenced by the disappeared Raman peaks of *o*-DCB (Figure S8, SI), after being heated up to room temperature, and finally after thermal annealing at 150 °C for 5 min. It is apparent that there is no observable difference between the Raman spectra before and after solvent removal via sublimation at −25 °C, suggesting that the orderly packed P3HT aggregates remain even without solvent. In contrast, after the heating back to room temperature, the Raman spectrum evolves into that of the sample prepared with direct drying plus postannealing, and the subsequent annealing of the freeze-dried sample does not alter the Raman spectrum further. This result shows good agreement with the corresponding absorption spectra: (1) the low-energy vibronic feature of the cooled P3HT:PCBM in *o*-DCB remains after drying, (2) the feature below 1.9 eV wanes upon heating to room temperature and it is compensated by the increased absorption feature above 2.2 eV, and (3) the subsequent thermal annealing only alters absorption slightly. This absorption spectrum is distinct from that of the sample prepared with direct drying plus postannealing, which exhibits a


DOI: 10.1021/acs.jpcc.7b01679
J. Phys. Chem. C 2017, 121, 14826−14834

higher-energy absorption edge.[7] One possible explanation to the above-mentioned spectral data is that the heating back to room temperature allows for increased entropic degrees of freedom—the randomness in the separation between adjacent chains and their mutual alignment, engendered by relaxation of molecular conformation—to further decrease the free energy of the system, thus reducing the interchain coupling and weakening the corresponding signatures of sharp red-shifted Raman peaks and low-energy vibronic feature in absorption. Is there only one benefit by fabricating P3HT:PCBM films with the freeze-drying method, i.e., more red-shifted absorption spectrum in the active layer? In fact, there is another great advantage with the freeze-drying method. Many trial-and-error efforts in the conventional direct thermal annealing method must be taken to search for the optimal fabrication condition in BHJ polymer solar cells, because removal of solvent molecules at high temperatures interferes with ordered stacking of polymers. On the other hand, the freeze-drying method separates the formation of ordered molecular aggregates from the solvent removal process.

As a note, the in situ spectroscopic studies were also performed on spin-coated solution films. No difference was recognized in the obtained experimental findings, except with a significantly weaker signal, indicating that spin-inducing shearing in the resultant films does not alter the short-range order within the ordered aggregates of P3HT. In light of the intermolecular coupling revealed by optical spectroscopy, can the characteristics of this short-range order shed light on long-range order on the nanometer scale, which is also important for the photovoltaic performance of BHJ polymer solar cells?

**GIXRD.** Long-range order of materials is best characterized with X-ray scattering methods. Two-dimensional grazing-incident X-ray diffraction (2D GIXRD) patterns of the freeze-dried and conventionally direct-dried P3HT:PCBM films with and without thermal annealing treatment at 150 °C are displayed in parts a, b, and c of Figure 6, respectively. Several features are noticeable from the results. Compared with prominent diffraction features at (100), (200), and (300) in the out-of-plane direction of neat freeze-dried P3HT films (Figure S9, SI), the blurry spots at these directions of P3HT:PCBM films signify less lamellar ordered structure, possibly owing to the interference by the dispersed PCBM molecules during further crystallization in the drying process. In contrast, the mixing of PCBM into P3HT does not alter either the spectra of Raman scattering or absorption of frozen solution, suggesting that P3HT and PCBM aggregated separately in the solution and did not affect each other. Furthermore, the clearly isotropic broad ring shape with a maximum at ~1.36 $Å^{-1}$ is the PCBM halo peak due to clustering of PCBM molecules,[34] qualitatively indicating more PCBM aggregation on a molecular scale for both the freeze-dried films with and without post-annealing compared to the direct-dried film. Finally, the brighter diffraction spots at (100), (200) and (300) of the freeze-dried P3HT:PCBM film (Figure 6b) show that the freeze-dried film bears stronger P3HT crystallinity than the direct-dried film. The corresponding out-of-plane GIXRD profiles, shown in Figure 6d, provide more detailed illustration of the respective edge-on P3HT crystallites in three aspects. First, the (100) spot of the freeze-dried film (the red curve) resides at $Q_Z$ = 0.46 $Å^{-1}$, which is larger than that of the direct-dried film (the black curve, $Q_Z$ = 0.4 $Å^{-1}$), indicating more compact P3HT lamellar packing for the freeze-dried film. This shifted (100) spot of the freeze-dried film is correspondent to its shifted (200) spot.

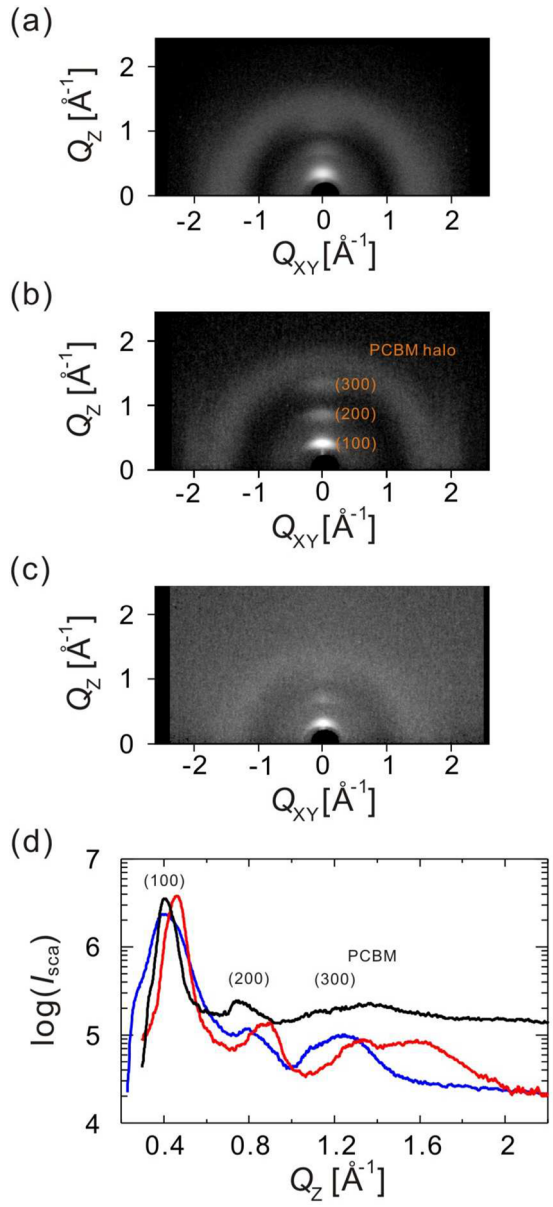


**Figure 6.** 2D GIXRD patterns of P3HT:PCBM (1:0.8) films on Si(111) substrates prepared by (a) freeze-drying as cast, (b) freeze-drying plus post-thermal annealing, and (c) direct-drying plus post-thermal annealing both at 150 °C for 5 min. (d) Blue, red, and black curves are out-of-plane GIXRD profiles (reduced along the direction normal to the film surface and obtained by cake cut integrating over a ±30° angular range from above the photographs in parts a–c).

Second, the widths of the (100) spot of the two films (the red and black curves) are comparable, implying analogous P3HT domain size. Third, the less diffusive background in the diffraction profile of the freeze-dried film signifies more ordered P3HT domains. The GIXRD results show that there are more molecular-scale PCBM clusters in the pristine freeze-dried film, as shown in Figure 6d. The freeze-dried film with post-annealing has the slightly obvious PCBM halo peak compared to the freeze-dried film without post-annealing, suggesting that the PCBM aggregation enhanced by thermal effect is limited. In order to test the thermal stability of film morphology, the freeze-dried and direct-dried P3HT:PCBM thin films were heated to 150 °C for 30 min, and their scanning electron microscopic images (not shown here) signified that micron-



DOI: 10.1021/acs.jpcc.7b01679
J. Phys. Chem. C 2017, 121, 14826–14834

scale PCBM aggregates were absent in the freeze-dried films,[8] potentially offering greater device stability. Combining these results, a hypothesis then emerges to provide a possible explanation: the uniformly dispersed, precast small size of PCBM clusters (presumably on the nanometer scale and separated by ordered P3HT aggregates) in freeze-dried films hinders PCBM diffusion to form large aggregates after post-annealing.

Structural characterization of BHJ polymer solar cells has been usually carried out with various kinds of microscopic tools, e.g., scanning electron microscopy (SEM),[35,36] transmission electron microcopy (TEM),[36−39] and scanning probe microscopy (SPM) and its associated kinds.[35,36,39,40] The provided information has facilitated the development of processing approaches to improve photovoltaic performance, including efficiency and stability. However, the two electron microscopic tools are limited by their spatial resolution and imaging contrast of organic molecules to resolve molecular packing that is relevant to the charge transport in organic electronic devices, while scanning probe microscopic tools are restricted to surface characteristics. Optical spectroscopic methods (Raman scattering, absorption, and photoluminescence), on the other hand, probe vibrational modes and electronic transitions of organic materials that are sensitive to intermolecular interaction and therefore molecular packing. In comparison, although X-ray diffraction confers a packing configuration, it only reveals the lattice spacing of crystalline materials, but it is blind to amorphous aggregates that are common in BHJ blended systems. Namely, the optical probes reveal indirect, but relevant, local packing order between adjacent molecules in organic blends, while X-ray diffraction exposes corresponding long-range order. The molecular packing order thus disclosed is beyond the reach of SEM, TEM, and SPM methods, if not impossible to distinguish.

## CONCLUSIONS

In conclusion, in situ spectroscopy of Raman scattering, absorption, and photoluminescence were used to monitor the progression of the P3HT molecular stacking in either pristine P3HT or P3HT:PCBM blends dissolved in *o*-DCB during the freeze-drying process. The results of Raman spectroscopy show that P3HT polymers undergo drastic ordered aggregation upon being lower than 0 °C, at which the solubility of P3HT is reached, as evidenced by the emergence of pronounced red-shifted narrow Raman peaks caused by extended conjugation and intermolecular coupling. Disordered P3HT was identified unequivocally during the course, thanks to the well-behaved spectral propensity of Raman peaks. The Raman data display great correspondence to the results of absorption and photoluminescence. They were further confirmed by coarse-grained molecular dynamic (MD) simulation, with which the order parameters of distance and orientation between P3HT chains exhibit enhancement upon cooling. While optical spectroscopy and MD simulation portrayed the short-range order of P3HT aggregates from the spectral evolution of Raman scattering, absorption, and photoluminescence, grazing-incident X-ray diffraction exposed the long-range order from the pronounced diffraction spots corresponding to the lamellar stacking of P3HT and PCBM clustering. Precast P3HT ordered aggregates and PCBM clusters created by dynamically cooling are preserved via sublimation. This study shows how the freeze-drying method attains good control in ordered molecular stacking without resorting to trial and error in fabricating bulk heterojunction polymer solar cells and also demonstrates the ability of Raman spectroscopy in quantitatively revealing the short-range order of polymer packing.

## ASSOCIATED CONTENT

### Supporting Information

The Supporting Information is available free of charge on the ACS Publications website at DOI: 10.1021/acs.jpcc.7b01679.

Schematic of the experiment setup; Raman, absorption, and PL spectra at finer temperature changes; peak assignments of Raman spectra; schematic illustrations of $f_{RDF}(r_{TP})$ and orientational order parameter $S$; CGMD simulations; full Raman spectra of P3HT:PCBM solution before and after sublimation; GIXRD profiles of neat P3HT films (PDF)

## AUTHOR INFORMATION


### Corresponding Authors

*C.-W.P. e-mail: cwpao@gate.sinica.edu.tw.
*C.-S.T. e-mail: cstsao@iner.gov.tw.
*J.-K.W e-mail: jkwang@ntu.edu.tw.

### ORCID

Yu-Bing Lan: 0000-0001-5276-0149


### Notes

The authors declare no competing financial interest.

## ACKNOWLEDGMENTS

The authors acknowledge Prof. Wei-Fang Su and her group at National Taiwan University for helping measuring GIXRD with an X-ray scattering system (Nanostar, Bruker) and thank Dr. Chao-Han Cheng's participation in early discussions and Dr. Feng-Cheng Hsu's initial effort of setting the laser spectroscopy instrument used in this study. The financial support is provided by Ministry of Science and Technology (102-2112-M-002-011-MY3) and Academia Sinica (AS-103-SS-A02) at Taiwan.

## REFERENCES


(1) Hains, A. W.; Liang, Z.; Woodhouse, M. A.; Gregg, B. A. Molecular Semiconductors in Organic Photovoltaic Cells. *Chem. Rev.* **2010**, *110*, 6689−6735.

(2) Kippelen, B.; Bredas, J.-L. Organic Photovoltaics. *Energy Environ. Sci.* **2009**, *2*, 251−261.

(3) Goedkoop, M.; Spriensma, R. *The Eco-indicator 99: A Damage Oriented Method for Life Cycle Impact Assessment: Methodology Report*; PRé Consultants B.V.: LE Amersfoort, The Netherlands, 2001.

(4) Gong, J.; Darling, S. B.; You, F. Perovskite Photovoltaics: Life-cycle Assessment of Energy and Environmental Impacts. *Energy Environ. Sci.* **2015**, *8*, 1953−1968.

(5) Yu, G.; Gao, J.; Hummelen, J. C.; Wudl, F.; Heeger, A. J. Polymer Photovoltaic Cells - Enhanced Efficiencies via a Network of Internal Donor-acceptor Heterojunctions. *Science* **1995**, *270*, 1789−1791.

(6) Ma, W. L.; Yang, C. Y.; Gong, X.; Lee, K.; Heeger, A. J. Thermally Stable, Efficient Polymer Solar Cells with Nanoscale Control of the Interpenetrating Network Morphology. *Adv. Funct. Mater.* **2005**, *15*, 1617−1622.

(7) Li, G.; Yao, Y.; Yang, H.; Shrotriya, V.; Yang, G.; Yang, Y. "Solvent Annealing" Effect in Polymer Solar Cells Based on Poly(3-hexylthiophene) and Methanofullerenes. *Adv. Funct. Mater.* **2007**, *17*, 1636−1644.

(8) Huang, P.-T.; Chou, C.-W.; Lin, B.-Y.; Shi, Z.-E.; Huang, Y.-J.; Chen, C.-T.; Cheng, C.-H.; Wang, J.-K. Controlling the Morphology of Poly(3-hexylthiophene)/Methanofullerene Film through a Dynamic-cooling and Freeze-drying Process. *Polym. Int.* **2016**, *65*, 66−71.




DOI: 10.1021/acs.jpcc.7b01679
*J. Phys. Chem. C* 2017, 121, 14826−14834

(9) Balkanski, M.; Wallis, R. F.; Haro, E. Anharmonic Effects in Light-scattering due to Optical Phonons in Silicon. *Phys. Rev. B: Condens. Matter Mater. Phys.* **1983**, *28*, 1928−1934.
(10) Zen, A.; Saphiannikova, M.; Neher, D.; Grenzer, J.; Grigorian, S.; Pietsch, U.; Asawapirom, U.; Janietz, S.; Scherf, U.; Lieberwirth, I.; et al. Effect of Molecular Weight on the Structure and Crystallinity of Poly(3-hexylthiophene). *Macromolecules* **2006**, *39*, 2162−2171.
(11) Huang, Y.-C.; Tsao, C.-S.; Chuang, C.-M.; Lee, C.-H.; Hsu, F.-H.; Cha, H.-C.; Chen, C.-Y.; Lin, T.-H.; Su, C.-J.; Jeng, U. S.; et al. Small- and Wide-angle X-ray Scattering Characterization of Bulk Heterojunction Polymer Solar Cells with Different Fullerene Derivatives. *J. Phys. Chem. C* **2012**, *116*, 10238−10244.
(12) Lee, C.-K.; Pao, C.-W.; Chu, C.-W. Multiscale Molecular Simulations of the Nanoscale Morphologies of P3HT:PCBM Blends for Bulk Heterojunction Organic Photovoltaic Cells. *Energy Environ. Sci.* **2011**, *4*, 4124−4132.
(13) Lee, C. K.; Hua, C. C.; Chen, S. A. Phase Transition and Gels in Conjugated Polymer Solutions. *Macromolecules* **2013**, *46*, 1932−1938.
(14) Phillips, J. C.; Braun, R.; Wang, W.; Gumbart, J.; Tajkhorshid, E.; Villa, E.; Chipot, C.; Skeel, R. D.; Kale, L.; Schulten, K. Scalable Molecular Dynamics with NAMD. *J. Comput. Chem.* **2005**, *26*, 1781−1802.
(15) Gao, Y.; Grey, J. K. Resonance Chemical Imaging of Polythiophene/Fullerene Photovoltaic Thin Films: Mapping Morphology-dependent Aggregated and Unaggregated C═C Species. *J. Am. Chem. Soc.* **2009**, *131*, 9654−9662.
(16) Tsoi, W. C.; James, D. T.; Kim, J. S.; Nicholson, P. G.; Murphy, C. E.; Bradley, D. D. C.; Nelson, J.; Kim, J.-S. The Nature of In-plane Skeleton Raman Modes of P3HT and Their Correlation to the Degree of Molecular Order in P3HT:PCBM Blend Thin Films. *J. Am. Chem. Soc.* **2011**, *133*, 9834−9843.
(17) Milani, A.; Brambilla, L.; Del Zoppo, M.; Zerbi, G. Raman Dispersion and Intermolecular Interactions in Unsubstituted Thiophene Oligomers. *J. Phys. Chem. B* **2007**, *111*, 1271−1276.
(18) Donohoo-Vallett, P. J.; Bragg, A. E. $\pi$-Delocalization and the Vibrational Spectroscopy of Conjugated Materials: Computational Insights on Raman Frequency Dispersion in Thiophene, Furan, and Pyrrole Oligomers. *J. Phys. Chem. B* **2015**, *119*, 3583−3594.
(19) Louarn, G.; Trznadel, M.; Buisson, J. P.; Laska, J.; Pron, A.; Lapkowski, M.; Lefrant, S. Raman Spectroscopic Studies of Regioregular Poly(3-alkylthiophenes). *J. Phys. Chem.* **1996**, *100*, 12532−12539.
(20) Schmidt-Hansberg, B.; Sanyal, M.; Klein, M. F. G.; Pfaff, M.; Schnabel, N.; Jaiser, S.; Vorobiev, A.; Mueller, E.; Colsmann, A.; Scharfer, P.; et al. Moving through the Phase Diagram: Morphology Formation in Solution Cast Polymer-Fullerene Blend Films for Organic Solar Cells. *ACS Nano* **2011**, *5*, 8579−8590.
(21) Rohac, V.; Ruzicka, V.; Ruzicka, K.; Polednicek, M.; Aim, K.; Jose, J.; Zabransky, M. Recommended Vapour and Sublimation Pressures and Related Thermal Data for Chlorobenzenes. *Fluid Phase Equilib.* **1999**, *157*, 121−142.
(22) Griffing, V.; Cargyle, M. A.; Corvese, L.; Eby, D. Temperature Coefficients of Viscosity of Some Halogen Substituted Organic Compounds. *J. Phys. Chem.* **1954**, *58*, 1054−1056.
(23) Edward, J. T. Molecular Volumes and the Stokes-Einstein Equation. *J. Chem. Educ.* **1970**, *47*, 261−270.
(24) Clark, J.; Silva, C.; Friend, R. H.; Spano, F. C. Role of Intermolecular Coupling in the Photophysics of Disordered Organic Semiconductors: Aggregate Emission in Regioregular Polythiophene. *Phys. Rev. Lett.* **2007**, *98*, 206406.
(25) Panzer, F.; Sommer, M.; Baessler, H.; Thelakkat, M.; Köhler, A. Spectroscopic Signature of Two Distinct H-aggregate Species in Poly(3-hexylthiophene). *Macromolecules* **2015**, *48*, 1543−1553.
(26) Rahimi, K.; Botiz, I.; Agumba, J. O.; Motamen, S.; Stingelin, N.; Reiter, G. Light Absorption of Poly(3-hexylthiophene) Single Crystals. *RSC Adv.* **2014**, *4*, 11121−11123.
(27) Turner, S. T.; Pingel, P.; Steyrleuthner, R.; Crossland, E. J. W.; Ludwigs, S.; Neher, D. Quantitative Analysis of Bulk Heterojunction Films Using Linear Absorption Spectroscopy and Solar Cell Performance. *Adv. Funct. Mater.* **2011**, *21*, 4640−4652.
(28) Spano, F. C. The Spectral Signatures of Frenkel Polarons in H- and J-aggregates. *Acc. Chem. Res.* **2010**, *43*, 429−439.
(29) Spano, F. C.; Silva, C. H- and J-aggregate Behavior in Polymeric Semiconductors. *Annu. Rev. Phys. Chem.* **2014**, *65*, 477−500.
(30) Huang, D. M.; Faller, R.; Do, K.; Moule, A. J. Coarse-grained Computer Simulations of Polymer/Fullerene Bulk Heterojunctions for Organic Photovoltaic Applications. *J. Chem. Theory Comput.* **2010**, *6*, 526−537.
(31) Schwarz, K. N.; Kee, T. W.; Huang, D. M. Coarse-grained Simulations of the Solution-phase Self-assembly of Poly(3-hexylthiophene) Nanostructures. *Nanoscale* **2013**, *5*, 2017−2027.
(32) Collings, P. J.; Hird, M. *Introduction to Liquid Crystals*; Taylor & Francis: Bristol, 1997.
(33) Thompson, B. C.; Frechet, J. M. J. Organic Photovoltaics - Polymer-Fullerene Composite Solar Cells. *Angew. Chem., Int. Ed.* **2008**, *47*, 58−77.
(34) Gomez, E. D.; Barteau, K. P.; Wang, H.; Toney, M. F.; Loo, Y.-L. Correlating the Scattered Intensities of P3HT and PCBM to the Current Densities of Polymer Solar Cells. *Chem. Commun.* **2011**, *47*, 436−438.
(35) Hoppe, H.; Niggemann, M.; Winder, C.; Kraut, J.; Hiesgen, R.; Hinsch, A.; Meissner, D.; Sariciftci, N. S. Nanoscale Morphology of Conjugated Polymer/fullerene-based Bulk-heterojunction Solar Cells. *Adv. Funct. Mater.* **2004**, *14*, 1005−1011.
(36) Hoppe, H.; Sariciftci, N. S. Morphology of Polymer/fullerene Bulk Heterojunction Solar Cells. *J. Mater. Chem.* **2006**, *16*, 45−61.
(37) Brinkmann, M.; Rannou, P. Molecular Weight Dependence of Chain Packing and Semicrystalline Structure in Oriented Films of Regioregular Poly(3-hexylthiophene) Revealed by High-Resolution Transmission Electron Microscopy. *Macromolecules* **2009**, *42*, 1125−1130.
(38) van Bavel, S. S.; Loos, J. Volume Organization of Polymer and Hybrid Solar Cells as Revealed by Electron Tomography. *Adv. Funct. Mater.* **2010**, *20*, 3217−3234.
(39) Pfannmoeller, M.; Kowalsky, W.; Schroeder, R. R. Visualizing Physical, Electronic, and Optical Properties of Organic Photovoltaic Cells. *Energy Environ. Sci.* **2013**, *6*, 2871−2891.
(40) Giridharagopal, R.; Cox, P. A.; Ginger, D. S. Functional Scanning Probe Imaging of Nanostructured Solar Energy Materials. *Acc. Chem. Res.* **2016**, *49*, 1769−1776.


DOI: 10.1021/acs.jpcc.7b01679
*J. Phys. Chem. C* 2017, 121, 14826−14834